INSTITUTE OF PHYSICS PUBLISHING SUPERCONDUCTOR SCIENCE AND TECHNOLOGY

Supercond. Sci. Technol. **16** (2003) 857–864 PII: S0953-2048(03)58768-1

Hysteresis and relaxation in $TlBa_2Ca_2Cu_3O_y$ superconducting polycrystals

A J Batista-Leyva[1,2,5], R Cobas[2,3], M T D Orlando[4] and E Altshuler[2]

[1] Physics Department, Engineering Faculty, University of Holguín, Holguín 80100, Cuba
[2] Superconductivity Laboratory, IMRE-Physics Faculty, University of Havana, 10400 Havana, Cuba
[3] Group of New Materials, Brazilian Center of Physics Research, 22290-180 Rio de Janeiro, Brazil
[4] Physics Department, Universidade Federal do Espíritu Santo, Vitoria ES 29060-900, Brazil

E-mail: alfobatista@yahoo.com

Received 20 January 2003, in final form 21 May 2003
Published 2 July 2003
Online at stacks.iop.org/SUST/16/857

Abstract

We study the hysteresis and relaxation of both intragranular and intergranular properties of $TlBa_2Ca_2Cu_3O_y$ (Tl-1223) superconducting polycrystals between 80 and 120 K. The samples have been prepared using a technique involving the mixing of grains of different sizes before the final sintering. The grains show a sizeable reversible magnetization, while vortices inside the grain behave as three-dimensional objects. The transport critical current is strongly hysteretic, with features that distinguish our Tl-1223 samples from 'standard' $YBa_2Cu_3O_{7-\delta}$ (YBCO), $(Hg, Re)Ba_2Ca_2Cu_3O_{8+\delta}$ (HBCCO) and $(Bi, Pb)_2Sr_2Ca_2Cu_3O_{10-\delta}$ (BSCCO) polycrystals. The preparation method improves the transport properties of the samples. The relaxation of the transport critical current density, in the presence of trapped fields, is reported here for the first time in this system, as far as we know. A phenomenological model can qualitatively describe the transport properties, where the intragrain magnetization affects the intergranular junctions, but a precise quantitative description is not achieved. The differences in the shape of the transport measurements, for different polycrystalline systems, are also well described by the model.

1. Introduction

The irreversibility of intergranular properties has proven to be a powerful tool for understanding the overall behaviour of superconducting polycrystals. Müller and Mathews [1] and Altshuler *et al* [2] have developed a model based on the influence of the flux trapped inside the grains on the current-carrying capabilities of the weak links between grains to explain the irreversibility of transport properties in high-temperature superconductors (HTS). It has been successfully used to study $YBa_2Cu_3O_{7-\delta}$ (YBCO) [2], $(Bi, Pb)_2Sr_2Ca_2Cu_3O_{10-\delta}$ (BSCCO) [3] and $(Hg, Re)Ba_2Ca_2Cu_3O_{8+\delta}$ (HBCCO) [4] ceramics. As far as we know, the model has not been employed in $TlBa_2Ca_2Cu_3O_y$ (Tl-1223) ceramics for low magnetic fields. In [5] a model derived from the one we use here is applied to study of the hysteresis of transport critical current density in Tl-based composites in fields up to 1.5 T.

The model also explains the time variation (or relaxation) of transport properties in HTS, ascribing it as a resulting effect of the relaxation of the flux trapped inside the grains. Altshuler *et al* [6] and Cobas *et al* [7] used this approach to explain the relaxation of the transport critical current in YBCO and HBCCO HTS.

[5] Present address: Superconductivity Laboratory, University of Havana, PO Box 6631, La Habana 10600, Cuba.

In most previous papers, several parameters such as the first critical field (H_{c1g}) and saturation field of the grain (H^*) are extracted from transport measurements (i.e. from the so-called 'flux trapping' curve [8]). These parameters are then used to fit other intergranular experiments, such as the relaxation of the transport critical current.

We combine here both intragranular and intergranular measurements, through the use of magnetometric and transport techniques, respectively, in order to explain the irreversibility and the relaxation of the transport critical current density in Tl-1223 polycrystalline ceramics. The model gives a correct explanation of the observed phenomena, although a precise quantitative description is not achieved.

2. Experimental details

2.1. Samples

The superconducting polycrystals were prepared by the conventional precursor ceramic route. The precursor powder (without Tl) was prepared by mixing $SrCO_3$ (99.99%), $CaCO_3$ (99.99%) and CuO (99.99%), in stoichiometric proportions. The mixture was carefully milled and submitted to a heat treatment at 930 °C for 24 h at 1 atm of O_2 flux. This procedure was repeated three times. The x-ray powder diffraction analysis revealed that there was no trace of carbon compounds.

After the last procedure, the precursor was mixed with Tl_2O_3 in stoichiometric proportions. The final mixture powder was mounted inside a box built with gold foil. In order to obtain a high-density compound, the mixture was prepared with grains of three different sizes: 100, 60 and 20 μm. The same (1/3) mass proportion was used for each size. The gold box was introduced inside a carbon box, and this set-up was pressed and heated at the same time in an anvil pressure furnace. The pressure used to prepare the samples was 1 GPa and the temperature was 835 °C for 10 h.

2.2. Measurements

Magnetic measurements were carried out in a Quantum Design SQUID magnetometer MPMS-5S, in direct current (dc) mode, with a scanning length of 1 cm and ten scans per point to diminish noise. The field was applied along the longest dimension of the sample, after a zero-field cooling (ZFC) from a temperature higher than T_c, to the measurement temperature. Isothermal hysteresis loops were measured at a rate of 1 mT s^{-1}, up to a magnetic field greater than the irreversibility field, determined using a criterion of 25 A m^{-1}. Zero-field relaxation measurements were performed after a magnetic field greater than the field of total penetration ($H > H_{c1g} + 2H^*$) was applied, as recommended in [9].

The transport measurements were performed in an experimental set-up described elsewhere [10], and can be classified as follows.

- *Virgin curve*: After a ZFC, the magnetic field is increased at a constant rate, measuring at the same time the critical current density.
- *Returning curve*: After a ZFC, a maximum field, H_m, is applied, and then decreased at a constant rate, and the critical current density is measured simultaneously.

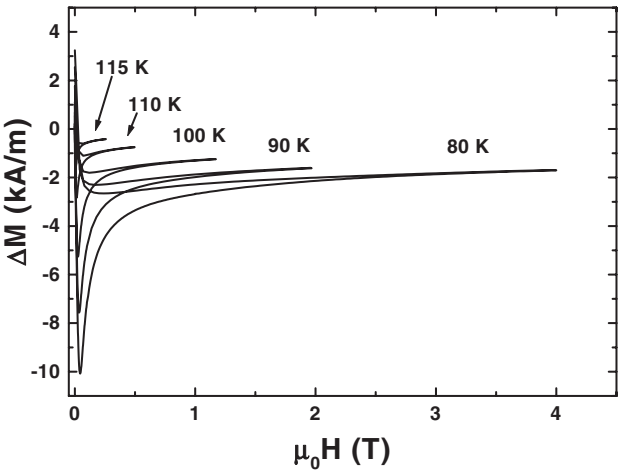

Figure 1. Isothermal magnetization loops at different temperatures.

- *Flux trapping curve*: After a ZFC, a maximum field is applied, and then removed. The critical current density is measured only in the remnant state. The procedure is repeated at different values of the maximum field. Applying a temperature higher than T_c erases the 'magnetic history' between consecutive values of H_m.
- *Relaxation of remnant critical current density*: After a ZFC, a maximum field is applied, and then removed. The critical current density in the remnant state is measured as a function of time, at a rate of one data point per second.

The measurements of the hysteresis of the transport critical current were performed as described in [4]. The relaxation of the transport critical current was measured following the procedure reported in [6].

3. Results and discussion

3.1. Magnetization measurements

The isothermal hysteresis loops for different temperatures are shown in figure 1. The presence of a sizeable reversible component is observed, revealed by the similarity of the slopes in the ascending and descending branches of each curve. No surface barriers are evident, because the descending branch is well below zero magnetization [9]. This shape in the magnetization curves was obtained in [11] and [12] for Hg1223 samples at temperatures close to the critical temperature. Both papers discuss the presence of surface barriers.

In figure 2 the first critical field (H_{c1g}), determined as the field for which the virgin curve departs from linearity, and the field for which the minimum magnetization is reached (H_{min}) are presented as a function of temperature. From these fields, it is possible to estimate the saturation field H^* of the grain as

$$H^* = H_{min} - H_{c1g}. \tag{1}$$

It is important to note that, as the magnetic fields applied in the measurement are large enough, all the magnitudes calculated are safely assumed to be intragranular.

The dependence of the width of the hysteresis loop with the inverse of the applied field (not shown here for brevity) increases its linearity as the temperature is increased. It could

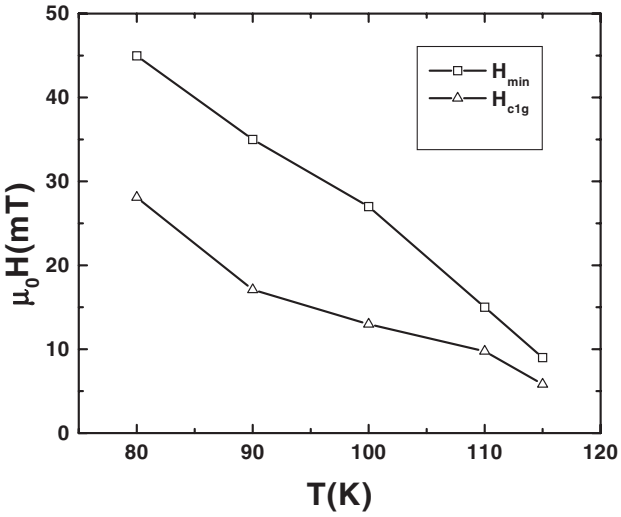

Figure 2. Temperature dependence of the first critical field and the field of minimum magnetization. The lines are to guide the eyes.

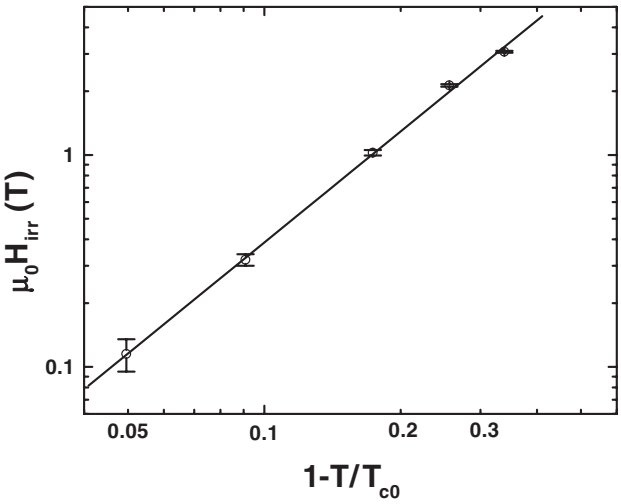

Figure 3. Intragranular irreversibility line from magnetometric experiments. The line is a guide to the eyes.

be a signature of the presence of weak surface barriers. But, if they were present, the values of H_{c1g}, or those of H_{min}, should be extracted from the slope of the dependence of the width of the hysteresis loop against the inverse of the applied field, assuming the theoretical result obtained in [13] must be

$$\Delta M \propto \frac{H_p^2}{H}. \qquad (2)$$

Here, H_p represents the penetration field–greater than the first critical field—due to the presence of surface barriers. Calculated values are far from those experimentally obtained, indicating that surface barriers do not seem to be the dominant pinning mechanism.

From the data in figure 1, it is possible to obtain the irreversibility line, represented in figure 3 in a log–log plot H_{irr} versus $(1 - T_{irr}/T_{c0})$. The slope gives the exponent n for the temperature dependence of this irreversibility field ($H_{irr} \sim (1 - T_{irr}/T_{c0})^n$). It is generally accepted that the values of n are related to the dimensionality of Abrikosov vortices. In particular, $n \approx 2$ implies they behave as three-dimensional (3D)

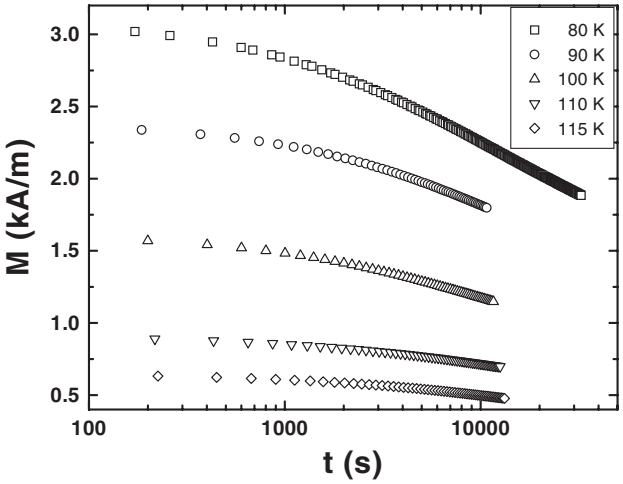

Figure 4. Time dependence of remnant magnetization at different temperatures.

flux lines [14, 15], while $n \approx 4$ has been associated with two-dimensional (2D) pancake vortices in Hg-1223 samples. In our sample, the slope (obtained from fitting the log–log graphic to a lineal model) is 2.05 ± 0.04, so we have evidence of 3D vortices in our Tl-1223 sample. Our result coincides with the value obtained in [16] for a Tl-1223/Ag composite, prepared by the powder-in-tube method. Glowacki [17] reports, for different composites, values that lie in the range of 2.0–2.3.

The 3D nature of the vortices is also justified by the dependence of the width of the magnetization loop with temperature, at a constant applied field (not shown here for brevity), which is clearly non-exponential, thus indicating that the vortices behave as 3D objects. Although evidence of a 2D–3D crossover in a Tl-2212 single crystal has been reported elsewhere at a temperature 7 K below T_c [18], in our case there is no evidence of such a crossover within a wide range of temperatures below T_c.

Figure 4 represents the time dependence up to 10 h of the remnant magnetization for different temperatures. In the semi-log plot of figure 4, our results clearly do not follow the relation (3), which differs from those obtained in [19], perhaps due to the fact that their measurements were performed in an applied field of 1 T. Different possible causes of nonlinearity are listed in [9]: the complexities of the remnant state, the redistribution of flux in the first stages of relaxation (obviously not our case), or the presence of collective pinning (associated with the movement of flux bundles, rather than isolated vortices). A common test for the last effect is to plot the time dependence of the relaxation rate. If the formula proposed by Feigel'man *et al* [20] for the description of the dependence of the intragranular critical current density with time (the so-called 'interpolation formula') holds, its signature should be a linear relation between $1/S_n$ and $\ln t$, while a power-law pinning barrier would produce a constant S_n value. In our case, the result departs from both behaviours; $1/S_n$ increases in an approximately linear way *with time*. So the observed nonlinearity could be related to the complexities of the flux distribution associated with the remnant state in the superconducting grains.

In order to obtain the effective intragranular pinning energy, and the normalized relaxation rates, the linear part

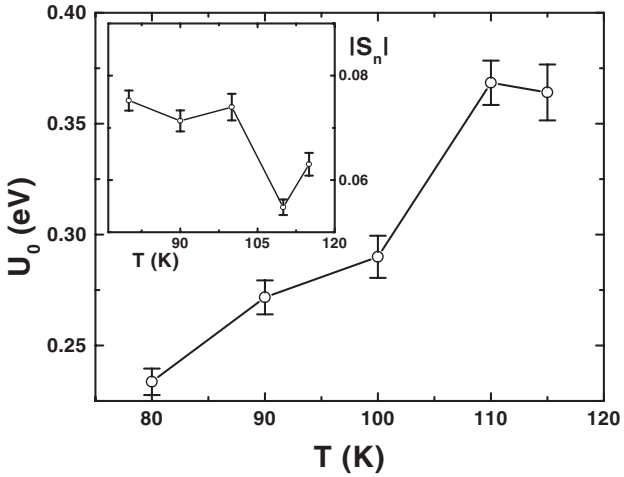

Figure 5. Temperature dependence of the effective intragranular pinning energy. In the inset, the temperature dependence of the absolute value of the normalized relaxation rate is shown. The lines are to guide the eyes.

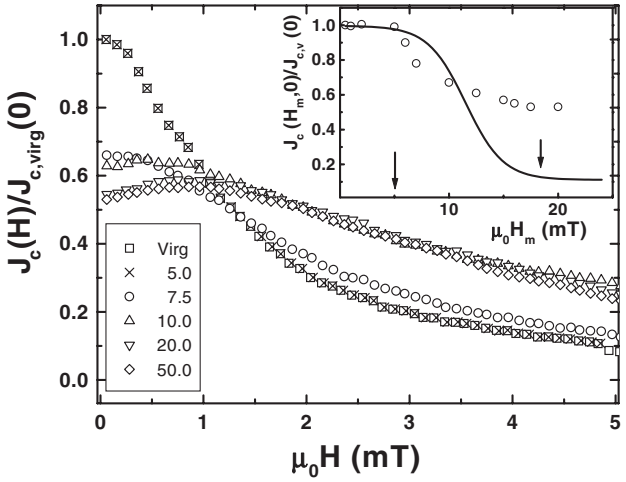

Figure 6. Virgin and returning curves at different maximum applied fields at 117 K. In the inset, the flux-trapping curve at this temperature is shown, with arrows indicating the first critical field (5 mT) and the saturation field (17.5 mT). In the legend, the maximum applied field is in mT.

of the experimental data is fitted by the expression [9]

$$M(t,T) = M_0(T)\left[1 - \frac{k_B T}{U_0(T)} \ln \frac{t}{\tau}\right] \tag{3}$$

where $M_0(T)$ is the initial magnetization at the absolute temperature T, $U_0(T)$ is the effective pinning energy of the Abrikosov vortices, k_B is the Boltzmann constant, t is the elapsed time from the beginning of relaxation, and τ is a characteristic time [20] which depends on the size of the sample (with typical values in the range 10^{-12}–10^{-6} s). It is difficult to determine $M_0(T)$, so we will eliminate it, evaluating equation (4) in a finite time t_b:

$$M(t_b,T) = M_0(T)\left[1 - \frac{k_B T}{U_0(T)} \ln \frac{t_b}{\tau}\right]. \tag{4}$$

The relaxation rate and the irreversible magnetization can be obtained from the experimental data, allowing us to calculate the normalized relaxation rate S_n as

$$S_n = \frac{1}{M_{irr}} \frac{dM}{d\ln(t)}. \tag{5}$$

Then, the pinning energy is calculated from equation (6) [9]

$$U_0 = k_B T \left\{-\frac{1}{S_n} + \ln \frac{t_b}{\tau}\right\} \tag{6}$$

which differs from the 'classical' Anderson–Kim expression, and is equivalent to it if the temperature is low enough.

Figure 5 shows the calculated values of U_0 as a function of temperature. In the inset, the temperature dependence of $|S_n|$ is represented. The overall trend of the curve is a monotonic decrement (increment) of $|S_n|$ (U_0), which is commonly reported at high temperatures [21]. However, for temperatures above 110 K an increment (small decrement) is observed. The behaviour of the curves for high temperatures could be an indication of the presence of a second peak, similar to that observed in [21], but there are not enough experimental points in our data to establish its existence. Against this supposition, though, speaks the vicinity of the irreversibility temperature. Further experimental work in this region of temperatures is necessary, in order to clarify the real nature of this effect.

3.2. Transport measurements

Figure 6 shows the virgin and several returning curves, measured at the temperature of 117 K. Some features of the curves must be underlined, as follows.

(i) The returning curves for $\mu_0 H_m \leqslant 5$ mT reproduce exactly the shape of the virgin curve.
(ii) The returning curves present maxima, and the field value at which each maximum is attained (H_{peak}) increases slightly with H_m.
(iii) There is a saturation field, H_m^{sat}, such that for $H_m \geqslant H_m^{sat}$ the returning curves almost overlap.
(iv) The values of $J_c(H_m, 0)$ (i.e. the remnant critical current density of the returning curves) are weakly dependent on H_m when compared with those for YBCO, HBCCO and BSCCO compounds.

The first three points are common to all ceramics previously measured with this technique. The fourth point is distinctive of this sample, and has not been found in previous measurements of other superconducting ceramics. This is coincident with the small decrement observed in the flux-trapping curve (shown, for $T = 117$ K, in the inset of figure 6), and has the same cause. Our result is closely related to that of [5]; they measured a Tl-1223/Ag composite for high fields $\mu_0 H_m \leqslant 1.5$ T, and found the remnant critical current density to be independent of the maximum applied field.

The parameters needed for the theoretical calculations within our model were obtained from figure 1 (H_{c1g} and H^*) and from the magnetic relaxation measurements (U_0). Finally, $\Gamma(G)$ the statistical distribution of geometrical factors to account for the compression or the decompression of flux in the intergranular region) was chosen to be triangular [2, 4], in such a way that the mean value was given by the following equation [4]:

$$\langle G \rangle = 2\frac{H_{peak}}{H^*}. \tag{7}$$

In YBCO [2] and HBCCO [4] ceramics, the peak value is far from zero (between 0.2–0.4), so $\langle G \rangle > 0$, while in BSCCO ceramics [3, 4] $H_{peak} \approx 0$, so $\langle G \rangle \approx 0$.

There is discussion in the literature regarding the shape and the mean value of $\Gamma(G)$. In [3, 22], the fact that for BSCCO the mean value is located close to zero is related to the tendency of grains in this material to plate-like growth, with the *c*-axis perpendicular to the flat side of the grains, and staked together. These grains form a dense conglomerate, as assumed in the brick wall model [23], which implies that there are situations of compression and decompression of magnetic flux, more or less equally distributed from the statistical point of view. So, the distribution of geometrical factors must include negative as well as positive values, with the mean value close to zero. But in [4], a BSCCO ceramic with needle-like grains without any stacking—as shown in scanning electron microscopy (SEM) micrographs—is studied, and the shape of returning curves and, consequently, the calculated statistical distribution of G are analogous. This suggests that there are other factors influencing G beyond grain morphology.

As can be seen from the inset in figure 6, the model only reproduces the presence of the first critical field (associated with the end of the first plateau) and the saturation of the grain, (associated with the beginning of the second plateau). Experimental values, obtained from transport measurements, are indicated by arrows in the inset of figure 6, and are approximately equal to the corresponding values extracted from figure 2, which were employed in theoretical calculations. This indicates that transport measurements in Tl-1223 polycrystals give a correct estimate of these intragranular parameters.

Similar disagreement between theory and experiment was found in [4] for a Bi-2223 sample, although, in our opinion, the causes are different. In the present case, a possible reason is the method of preparation (especially the mixing of different-sized grains), which creates strong percolative paths that are moderately affected by the applied field. This is why the decrement in the value of the critical current density, relative to its value at zero applied field, is less than 50%, while the model predicts about 90%.

Another picture of the same phenomenon can be obtained by measuring the resistive transition of the ceramic, in the presence of an applied magnetic field. Figure 7 represents this dependence for different field values. It can be seen that there is a change of behaviour for fields greater than 10 mT: the linearity of the curves measured for low fields is lost, and the curvature grows with the applied field.

In order to determine the magnitude of the intergranular effective pinning energy, a fit was carried out using the Arrhenius expression

$$\rho = \rho_0 \exp\left\{-\frac{U_0(H,T)}{k_B T}\right\} \tag{8}$$

with

$$U_0(H,T) = U(H)\left(1 - \frac{T}{T_{c0}}\right) \quad \text{for} \quad H < 10\,\text{mT} \tag{9}$$

$$U_0(H,T) = U(H)\left(\frac{T_{c0}}{T} - 1\right) \quad \text{for} \quad H \geqslant 10\,\text{mT}. \tag{10}$$

These two expressions for $U_0(H, T)$ account for the fact that dissipation is less temperature-dependent with the

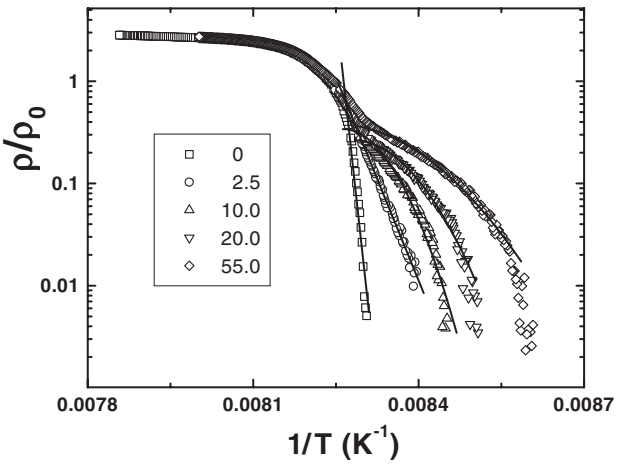

Figure 7. Arrhenius plots of the resistive transition at different applied fields. Lines follow the model described in the text. In the legend, the applied field is in mT.

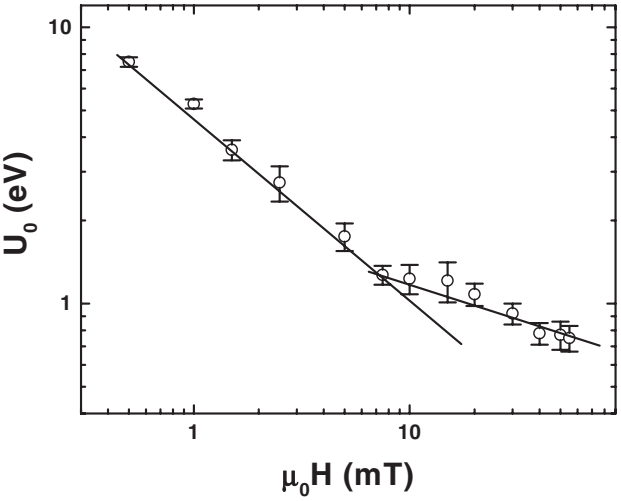

Figure 8. Field dependence of the effective intergranular pinning energy calculated from the resistive transition data. The lines are a fit to a linear model.

increment of the applied field. These results reflect the quality of the material for current transport.

An interesting feature of the above relations for the field and temperature dependence of the pinning energy is that, at 10 mT, there is a mismatch in $U_0(H, T)$. For the measurements performed in the present paper, where H is fixed while T varies, this mismatch has no great consequences. But for magnetoresistance measurements, where the temperature is fixed and the field varies, it implies that $U_0(H, T)$ will have a discontinuity proportional to T/T_{c0}. Further experimental work is needed in the region around the change of slope in $U(H)$ (see below) in order to clarify this discrepancy.

In figure 8, the field dependence of the effective pinning energy is shown. The change of behaviour is evident: the slope of the dependence diminishes, with the pinning energy less field-dependent for fields greater than 10.0 mT.

There is a coincidence that does not seem to be hazardous; the change of behaviour is attained when the magnetic field has a value for which, at the temperature of zero resistance, the external field reaches the first critical field value. So,

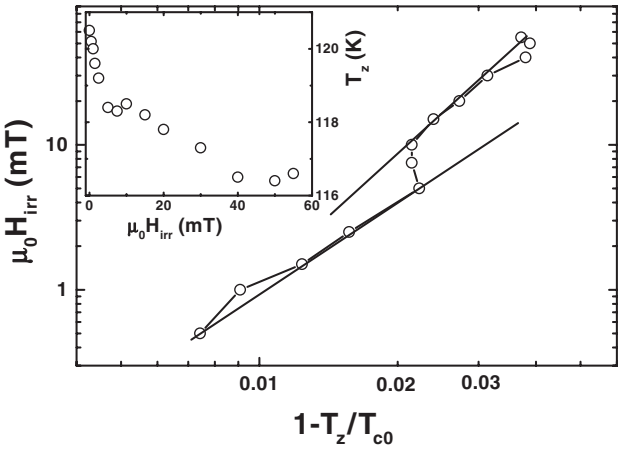

Figure 9. Intergranular irreversibility line calculated from transport experiments. The lines are a fit to a linear model. The original data are shown in the inset.

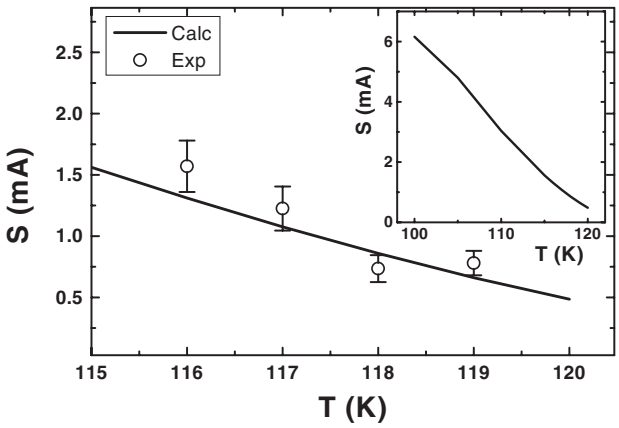

Figure 10. Temperature dependence of the remnant critical current relaxation rate, for a maximum applied field greater than that of saturation. The line follows the theoretical model described in the text. In the inset, this line is shown in a wider temperature window.

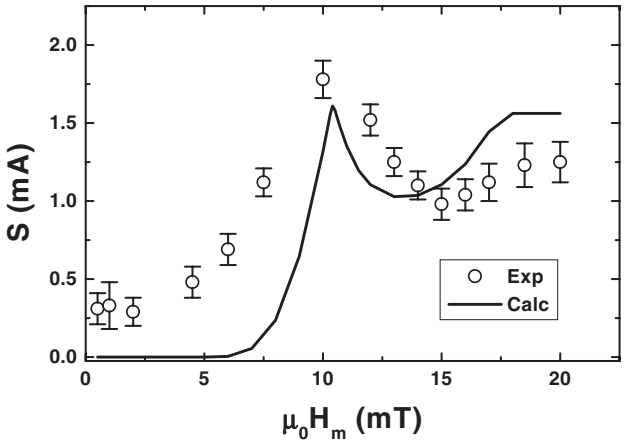

Figure 11. Maximum field dependence of the remnant critical current relaxation rate at the temperature of 117 K. The line is a fit to the theoretical model described in the text.

the combination of trapped and applied fields changes the dissipation regime. Equation (9) is valid in the field and temperature window where the field is expelled from the grains.

Figure 9 represents the intergranular irreversibility line, defined as the locus ($H_{\rm irr}$, $T_{\rm z}$), where $T_{\rm z}$ is the so-called *zero resistance critical temperature*, associated with the onset of dissipation in polycrystalline materials [24] (the original data are shown in the inset). The change of slope for higher fields (from 2.2 to 2.8) is also accompanied by a higher position of the line, i.e. the irreversible region is bigger. Straight lines are obtained via a linear regression.

Two types of measurements of the relaxation of the critical current density were performed: first, the dependence of the non-normalized relaxation rate with temperature, for a maximum field that guarantees the magnetic saturation of the grains (50 mT), and, secondly, the dependence of the relaxation rate with the maximum applied field, for a constant temperature. In all cases, the curves of the critical current density versus ln t are straight lines, with positive slopes. This fact is easy to understand, since flux creep inside the grains provokes the decrement of effective intergranular field acting on the weak link network, then enhancing the critical current as time passes.

Figure 10 shows the results of the first kind of relaxation measurement, as well as the fit by the theoretical model of [6] (the theoretical curve in a wider temperature window is shown in the inset). The agreement is good, at least in the small window of our experimental results. Measurements could not be performed at lower temperatures, because the current was too high and the current leads broke easily.

Figure 11 shows the dependence of the relaxation rate with the maximum field, at 117 K. The most remarkable features of the dependence are:

- there is a maximum at $\mu_0 H_{\rm m} = 10.0\,{\rm mT}$;
- there is a plateau for $\mu_0 H_{\rm m} < 6.0\,{\rm mT}$, with $S > 0$;
- for $\mu_0 H_{\rm m} > 15.0\,{\rm mT}$, there is again an increment of the relaxation rate;
- for $\mu_0 H_{\rm m} > 18.5\,{\rm mT}$, there is a second plateau.

Only one paper has reported on this behaviour in the literature, as far as we know: that published by Altshuler *et al* [6] for YBCO and HBCCO polycrystals. However, the shape of the curves in [6] has some differences when compared to that presented here. In the former, a sharp peak was found, with a fast decrement after $H_{\rm max}$, and in some cases there was a slight increment of the relaxation rate after the maximum.

Regarding the quality of the fit, it is comparable with that of [6]. The overall shape of the curve is well described, including the position of the maximum, the end of the first plateau and the beginning of the second one, but the quantitative description is not so good. A remarkable fact is the non-zero value of the relaxation rate for fields below the first critical field of the grains; if there is no trapped flux, it cannot relax at all! The possible reason of this discrepancy could be the presence of flux trapped in the intergranular region, which, in principle, can relax, and is not included in our model.

Let us further discuss the difference in shapes between figure 11 and its equivalent in [6] measured on YBCO and Hg-1223 polycrystals. For this, calculations were performed, using the model described here, of the dependence of the relaxation rate with the maximum applied field, when varying

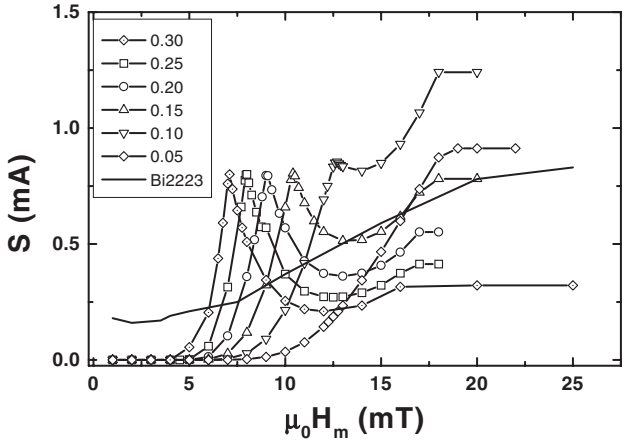

Figure 12. Theoretical dependence of the remnant critical current relaxation rate on the maximum field for different values of the mean geometrical factor G. The solid line represents the experimental result for a Bi-2223 sample.

the mean value of the geometrical factor, $\langle G \rangle$. The results are shown in figure 12. The decrease in $\langle G \rangle$ provokes a remarkable variation in the shape of the curve; for large geometrical factors, the curves show a sharp maximum, with an important decrement in S at the right of the peak. While $\langle G \rangle$ decreases, the maximum loses sharpness, and the decrement is less important. For low enough values of $\langle G \rangle$, the maximum does not appear and the curve has a monotonic increment until it reaches the final plateau.

The influence of $\langle G \rangle$ on the dependence of S with H_m can be understood as follows. The increment of H_m provokes an increment in the flux trapped inside the grains, so the relaxation should be more intense. But, at the same time, for the largest values of $\langle G \rangle$, the effective field acting on the junctions will be also large, so it will influence their current carrying capabilities. The combination of these two effects means that, initially, the relaxation rate will increase with the increment of the maximum applied field, and then it will diminish; this is why the maximum appears. For lower values of $\langle G \rangle$, in contrast, although there could be much flux trapped, its overall influence on the intergranular field will be small, so its influence on the junctions will be lower. This makes the fall of S less abrupt at the right of the maximum. For values close to zero, its effect will be so small that we will just find a monotonic increment of the relaxation rate, which saturates when the field trapped by the grains does.

This is exactly what we find in the experimental curves. For YBCO [2] and HBCCO [4], the curves show sharp maxima, while Tl-1223 presents a broader maximum. Finally, for BSCCO, whose dependence is also shown in figure 14 [25], there is no maximum. The values of $\langle G \rangle$ associated with these compounds, based on the results obtained for the hysteresis of critical current densities, diminish exactly in this order. While for the first two families a value between 0.2 and 0.4 is usually reported, here we have used 0.10 for Tl-1223 and, finally, for BSCCO a value very close to zero is typically used. The coincidence is remarkable, and reinforces the importance of geometrical factors for the interpretation of transport experiments in HTS.

4. Conclusions

Our measurements of the magnetization loops and the relaxation of the remnant magnetization between 80 K and the critical temperature in Tl-1223 polycrystals have shown that the magnetization of the grains has an important reversible component, and the Abrikosov vortices behave as 3D objects. The dynamics of these vortices influences the current carrying capabilities of the weak links between grains, showing their effect on the hysteresis of the transport critical current density. In the low magnetic field and high-temperature window studied, the hysteresis is not very pronounced, and the dependence of the remnant critical current density with the maximum applied field is less evident than for other HTS ceramics previously studied with the same experimental technique. These particularities seem to be related with the preparation method, which is believed to create strong percolative paths in the polycrystal. Measurements of resistivity versus temperature corroborate this statement. This preparation method could then constitute a way to improve transport properties in superconducting polycrystals.

Regarding the relaxation of the remnant critical current density in our samples, the comparison of the experimental results with the published reports found in the literature shows some differences, that are well accounted for by an intragranular flux trapping model, although its quantitative performance is not as good. The correspondence between the magnetic parameters determined via magnetometric measurements and the same determined using transport measurements is very good, as was found for other compounds in previous works. The influence of the effective demagnetization factor of the superconducting grains on the intergranular hysteresis and relaxation of transport properties is shown to be very important, so it is necessary to gain a deeper understanding of its relation with the morphology and properties of the grains.

Acknowledgments

This work was partially supported by TWAS grant no 95-124 RG/PHYS/LA and by the University of Havana 'Alma Mater' grant. We acknowledge bibliographical support from the ACLS/SSRC Working Group on Cuba.

References

[1] Müller K H and Mathews D N 1993 *Physica* C **206** 275–84
[2] Altshuler E, Musa J, Barroso J, Papa A R R and Venegas V 1993 *Cryogenics* **33** 308–13
[3] Muné P, Altshuler E, Musa J, García S and Riera R 1994 *Physica* C **226** 12–6
[4] Batista-Leyva A J, Cobas R, Estévez-Rams E, Orlando M T D, Noda C and Altshuler E 2000 *Physica* C **331** 57–66
[5] List F A, Kroeger D M and Selvamanickam V 1997 *Physica* C **275** 220–30
[6] Altshuler E, Cobas R, Batista -Leyva A J, Noda C, Flores L E, Martínez C and Orlando M T D 1999 *Phys. Rev.* B **60** 3673–9
[7] Cobas R, Batista -Leyva A J, García S and Altshuler E 2002 *Physica* C **366** 117–22
[8] Altshuler E, García S and Barroso J 1991 *Physica* C **177** 61–6
[9] Yeshurun Y, Malozemoff A P and Shaulov A 1996 *Rev. Mod. Phys.* 68 911–49

[10] Flores L E and Martínez C 1996 *Cryogenics* **36** 705–7
[11] Reissner M 1997 *Physica* C **290** 173–87
[12] Altshuler E, Chu C W, Orlando M T D, Sin A, Batista-Leyva A J, Buntar V and Weber H W 2002 *Physica* C **371** 224–8
[13] Burlachkov L 1993 *Phys. Rev.* B **47** 8056–64
[14] Yamauchi H, Karppinen M, Fujinami K, Ito T, Suematsu H, Matsuura K and Isawa K 1998 *Supercond. Sci. Technol.* **11** 1006–10
[15] Wisniewski A, Puzniak R, Karpinski J, Hofer J, Szymczak R, Baran M, Sauerzopf F M, Molinski R, Kopnin E M and Thompson J R 2000 *Phys. Rev.* B **61** 791–8
[16] Tang H, Wang Y Z, Yang Z Q, Zhang C, de Boer F R, Qiao G W, Zhou S H, Peng H T and Hua L 1997 *Physica* C **282–287** 2111–2
[17] Glowacki B A 1997 *Cryogenics* **37** 609–13
[18] Kopylov V N, Togonidze T G and Schegolev I F 1992 *Physica* C **195** 379–82
[19] Kim Y C and Kim G C 1997 *Physica* C **279** 122–6
[20] Feigel man M V, Geshkenbein V B, Larkin A I and Vinokur V M 1989 *Phys. Rev. Lett.* **63** 2303–6
[21] Paulius L M, Almasan C C and Maple M B 1993 *Phys. Rev.* B **47** 11627–30
[22] Muné P, Altshuler E and Musa J 1995 *Physica* C **246** 55–60
[23] Bulaevskii L N, Clem J R, Glazman L I and Malozemoff A P 1992 *Phys. Rev.* B **45** 2545–8
[24] Batista-Leyva A J, Orlando M T D, Rivero L, Cobas R and Altshuler E 2003 *Physica* C **383** 365–73
[25] Batista-Leyva A J 2002 Unpublished results